FLUID-STRUCTURE COUPLING OF A LINEAR ELASTIC MODEL WITH A COMPRESSIBLE FLOW MODEL WITH MULTILEVEL TIMESTEPPING

Michael Herty[1], Siegfried Müller[1,2] and Aleksey Sikstel[1,3]

[1] Institut für Geometrie und Praktische Mathematik, RWTH Aachen
Templergraben 55, 52056 Aachen, Germany
herty, mueller, sikstel@igpm.rwth-aachen.de

Key words: Fluid-structure interaction, coupling conditions, linear elastic model, compressible flow

Abstract.

Modeling of cavitation phenomena requires the coupling of models for fluid and solid materials. For this purpose we employ a strategy based on the solution of coupled Riemann problems that has been originally developed for the coupling of two fluids. The coupling strategy has been established and validated in [1]. In this work we include a timestepping algorithm which allows for different timesteps in fluid and solid solvers. Furthermore, we perform numerical experiments simulating the interface between a plastic or steel structure and air.

1 Introduction

Cavitation erosion is caused in solids exposed to strong pressure waves developing in an adjacent fluid field. The knowledge of the transient distribution of stresses in the solid is important to understand the cause of damaging by comparisons with breaking points of the material. The modelling of this problem requires coupling of models for fluid and solid.

The coupling of hyperbolic models has been discussed analytically and numerically in many recent publications and we refer to [2] for a survey. Particular results for the coupling of Euler equations with Euler equations exist and have been studied e.g. in [3]. Numerical approaches have been proposed e.g. in [4, 5]. Coupling the dynamic requires to postulate conditions to be fulfilled at the interface for almost all times $t \geq 0$.

One common approach is to iterate the coupling condition in each time step solving alternately the fluid and the solid model as in [6]. Alternatively, one may use strategy based on the solution of coupled Riemann problems that has been developed and validated

1

in [1]. This concept has been exemplified for the coupling of a linear elastic structure with an ideal gas. The coupling procedure relies on the solution of a nonlinear equation. Existence and uniqueness of the solution have been proven. However, the timesteps for the solvers were synchronised and consequently a very small timestep was imposed in the fluid solver. In order to avoid redundancy and to improve computational efficiency, local timestepping methods were considered in [7]. We develop a multilevel local timestep (MLTS) algorithm in the adaptive Runge-Kutta discontinuous Galerkin (RKDG) solver [8]. By numerical simulations we will verify the improvement in the computational time without spoiling the accuracy.

2 Model

Consider a situation as in Figure 1 where an interface separates a material and a compressible gas. It is assumed that the interface remains unaffected by the interaction of a gas flow with a material structure [6], i.e. we do not account for deformation of the structure.

Structure model: we assume that the material properties are sufficiently well described by a linear elastic model:

$$\frac{\partial \overline{\mathbf{v}}}{\partial t} - \frac{1}{\overline{\rho}} \nabla \cdot \overline{\boldsymbol{\sigma}} = \mathbf{0}, \tag{1a}$$

$$\frac{\partial \overline{\boldsymbol{\sigma}}}{\partial t} - \overline{\lambda} (\nabla \cdot \overline{\mathbf{v}}) \mathbf{I} - \overline{\mu} \left(\nabla \overline{\mathbf{v}} + \nabla \overline{\mathbf{v}}^T \right) = \mathbf{0}. \tag{1b}$$

Here, the density of the material is denoted by $\overline{\rho}$ and assumed to be constant. The deformation velocities are $\overline{\mathbf{v}} = (\overline{v}_1, \ldots, \overline{v}_d)^T$, the stress tensor is denoted by $\overline{\boldsymbol{\sigma}} = (\overline{\sigma}_{ij})_{i,j=1,\ldots,d} = \overline{\boldsymbol{\sigma}}^T$, and the Lamé constants are $\overline{\lambda}, \overline{\mu} > 0$. Finally, the dilatation wave velocity and the shear wave velocity are $\overline{c}_1^2 := (2\overline{\mu} + \overline{\lambda})/\overline{\rho}$ and $\overline{c}_2^2 := \overline{\mu}/\overline{\rho}$, respectively. Due to the symmetry of the stress tensor $\overline{\boldsymbol{\sigma}}$, the system of equations (1) contains redundant equations. Those may be removed and the system can be written in the canonical form of a system of conservation laws, see equation (29) in the Appendix A of [1].
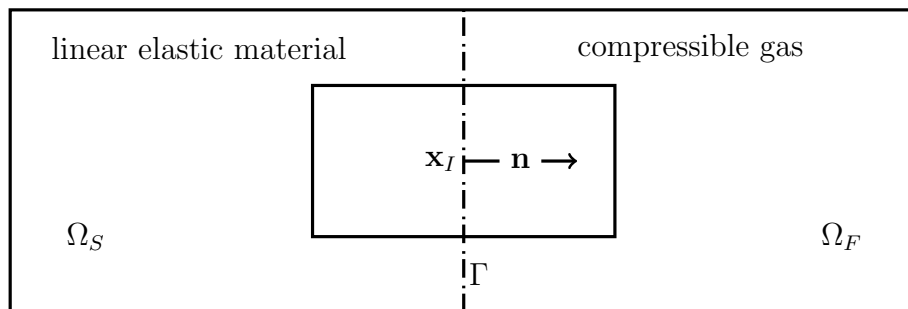
Figure 1: A sketch of the 2D problem with elastic material on the left and compressible gas on the right. Shown is the interface Γ (dashed) with its normal direction $\mathbf{n}$ starting at $\mathbf{x}_I \in \Gamma$ and two discretisation cells aligned with Γ. The coupling of the dynamics will be across the interface in normal direction.

Compressible model: in the compressible gas regime we assume that the dynamics are governed by Euler equations

$$\frac{\partial \rho}{\partial t} + \nabla \cdot (\rho \mathbf{v}) = 0, \tag{2a}$$

$$\frac{\partial \rho \mathbf{v}}{\partial t} + \nabla \cdot (\rho \mathbf{v}^T \mathbf{v} + p\mathbf{I}) = \mathbf{0}, \tag{2b}$$

$$\frac{\partial \rho E}{\partial t} + \nabla \cdot (\rho \mathbf{v}(E + p/\rho)) = 0, \tag{2c}$$

where we use the notation ρ for the gas density, $\mathbf{v} = (v_1, \ldots, v_d)^T$ for its velocity, E for the total energy $E = e + 0.5\mathbf{v}^2$, pressure p and internal energy e. The system is not closed and an equation of state is required for a complete description, see [9, 10]. Throughout this work we consider a perfect gas but emphasise that the overall concept extends to more general gas laws. For a perfect gas we have

$$p = (\gamma - 1)\rho e \tag{3}$$

and the speed of sound is given by

$$c = \sqrt{\frac{\gamma\, p}{\rho}}. \tag{4}$$

Here γ denotes the ratio of specific heats at constant pressure and volume, respectively.

Coupling: across the interface we couple the gas dynamics model (2) to the material model (1). To this end we project the equations onto the normal direction $\mathbf{n}$ of the interface. For notational convenience we assume the normal direction $\mathbf{n} = (n_i)_{i=1}^d$ pointing from the material towards the gas regime, see Figure 1. We project the linear elasticity model in $d \in \{1, 2, 3\}$ spatial dimensions onto direction $\mathbf{n} \in \mathbb{R}^d$ and obtain a quasi–1D model in the normal direction $x_n := \mathbf{n} \cdot \mathbf{x}$

$$\frac{\partial \overline{\mathbf{u}}}{\partial t} + \frac{\partial \overline{\mathbf{f}}_n(\overline{\mathbf{u}})}{\partial x_n} = \mathbf{0}, \quad \overline{\mathbf{f}}_n(\overline{\mathbf{u}}) := \sum_{i=1}^d \overline{\mathbf{f}}_i(\overline{\mathbf{u}}) n_i. \tag{5}$$

Here $\overline{\mathbf{u}}$ and $\overline{\mathbf{f}}_i$ are defined in Appendix A of [1]. The eigenvalues of the projected system (5), see equation (35) in the Appendix A of [1], are independent of the direction $\mathbf{n}$.

Similarly, we project the gas equations (2) onto $\mathbf{n}$. Provided there is no flow of gas in tangential directions $\tilde{x}_{i+1} = \mathbf{x} \cdot \mathbf{t}_i$, $i = 1, \ldots, d-1$, the system (2) reduces to the projected system:

$$\frac{\partial \tilde{\mathbf{u}}}{\partial t} + \frac{\partial \mathbf{f}_n(\tilde{\mathbf{u}})}{\partial x_n} = \mathbf{0}, \tag{6a}$$

$$\tilde{\mathbf{u}} := (\rho, \rho\tilde{\mathbf{v}}, \rho E)^T, \ \tilde{\mathbf{v}} := (\mathbf{n} \cdot \mathbf{v}, \mathbf{t}_1 \cdot \mathbf{v}, \ldots, \mathbf{t}_{d-1} \cdot \mathbf{v})^T, \ v_n := \mathbf{n} \cdot \mathbf{v}, \tag{6b}$$

$$\mathbf{f}_n(\tilde{\mathbf{u}}) := \sum_{i=1}^d \mathbf{f}_i(\tilde{\mathbf{u}}) n_i = \begin{pmatrix} \rho v_n \\ \rho v_n \tilde{\mathbf{v}} + p\mathbf{n} \\ \rho v_n(E + p/\rho) \end{pmatrix}, \tag{6c}$$

3

where $\mathbf{f}_i$ are defined in equation (40b) in Appendix B of [1]. Since both systems (5) and (6) are invariant under rotation and reflection, it is sufficient to consider the projection onto direction $\mathbf{n} = \mathbf{e}_1 = (1, 0, \ldots, 0)^T \in \mathbb{R}^d$, see Figure 1.

The basic problem is now to couple the projected systems at the interface Γ. The projected linear elastic model is defined in Ω_S and the projected Euler equations in Ω_F. Depending on the coupling conditions different wave patterns might be observed [11].

According to the transition conditions of continuum mechanics at a material interface we model the coupling by requiring the following conditions to be fulfilled at the interface:

$$\mathbf{n}^T \overline{\boldsymbol{\sigma}} \mathbf{n} \equiv \overline{\sigma}_{nn} \overset{!}{=} -p, \tag{7a}$$

$$\overline{\mathbf{v}}^T \mathbf{n} \equiv \overline{v}_n \overset{!}{=} v_n \equiv \mathbf{v}^T \mathbf{n}, \tag{7b}$$

neglecting viscosity and heat conduction in the gas flow. The conditions prescribe an equal stress and pressure at the interface. Also, we assume that across the interface the normal velocities are equal. The conditions (7) are referred to as transition and kinematic or coupling conditions, respectively.

The conditions (7) are used to provide boundary condition at some point $\mathbf{x}_I \in \Gamma$ of the interface for both the structure and the fluid. The procedure is described in Algorithm 1.

Algorithm 1 Coupling Conditions

1: Let $\overline{\mathbf{u}}_L = \overline{\mathbf{u}}(\mathbf{x}_I-, t)$ and $\mathbf{u}_R = \mathbf{u}(\mathbf{x}_I+, t)$ be the attached interfacial states for the structure and the fluid, respectively, at the interface point $\mathbf{x}_I \in \Gamma$ and time t.
2: Solve the coupled Riemann problem at $\mathbf{x}_I$ in normal interfacial direction $\mathbf{n}$ of the interface consisting of two half Riemann problems, i.e. find parameters ϵ^* and θ^* such that (7) holds for states $\overline{\mathbf{u}}(\epsilon) := \overline{\mathbf{L}}_1^+(\epsilon, \overline{\mathbf{u}}_L)$ on the forward Lax curve $\overline{\mathbf{L}}_1^+$ corresponding to the lowest characteristic speed in the structure and $\mathbf{u}(\theta) := \mathbf{L}_3^-(\theta, \mathbf{u}_R)$ on the backward Lax curve $\mathbf{L}_3^-$ corresponding to the fastest characteristic speed in the fluid.
3: Evaluate the Lax curves with respect to ϵ^* and θ^* to determine the boundary values $\overline{\mathbf{u}} = \overline{\mathbf{u}}(\epsilon^*)$ and $\mathbf{u} = \mathbf{u}(\theta^*)$ for the structure and the fluid, respectively.

Remark 2.1. *In [1] we proved that there exists a unique solution to the coupled Riemann problem in Step 2 of Algorithm 1 provided that the fluid state $\mathbf{u}_R$ is subsonic and, moreover, the initial states $\overline{\mathbf{u}}_L$ and $\mathbf{u}_R$ satisfy some constraint given in Theorem 3.1 of [1].*

3 Multilevel Timestepping

Depending on the material parameters the wave speeds in the solid may become significantly higher than in the fluid. Since the governing equations are hyperbolic a smaller time step for the solid solver is required provided an explicit scheme is used for time discretisation. In previous work [1] computations were performed synchronising the fluid and the solid solver by setting the minimum of the timesteps globally. This approach
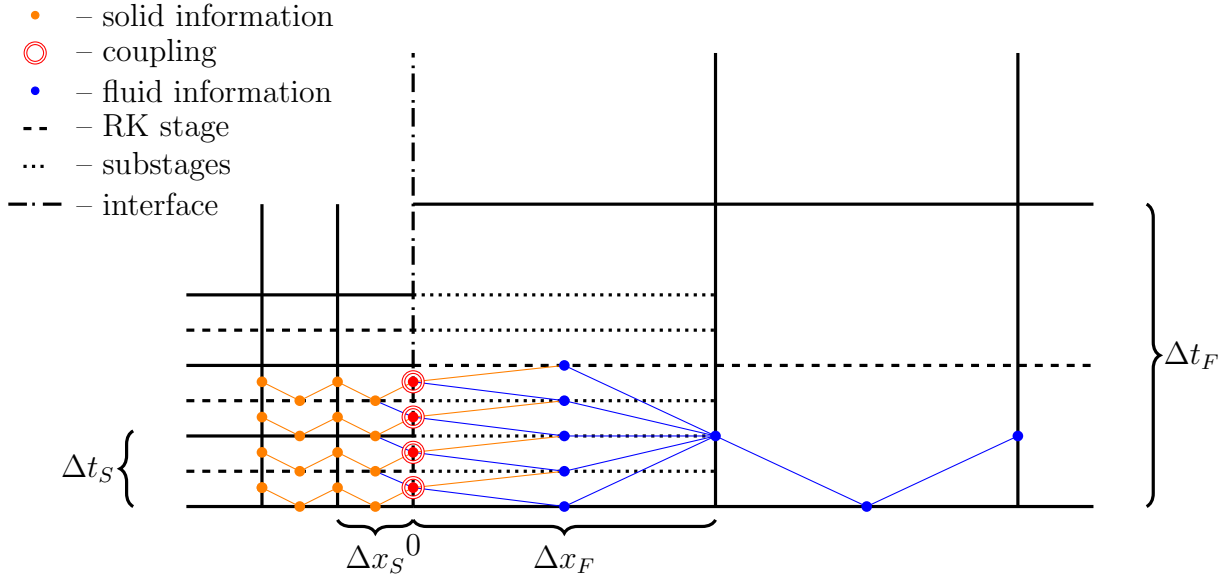
Figure 2: Sketch of MLTS. Δx_S and Δx_F represent the cell size, Δt_S and $\Delta t_F \gg \Delta t_S$ the timesteps. Subscripts $_S$ and $_F$ indicate solid and fluid, respectively.

entails a large amount of superfluous time steps in the fluid solver. For instance, the sound speed in stainless steel is approximately $5790\frac{m}{s}$ while in air merely $343\frac{m}{s}$, thus 4 out of 5 timesteps in the fluid solver might be redundant.

The timestepping is executed by means of explicit Runge-Kutta (RK) schemes with M_S stages in the solid part and M_F stages in the fluid part with nodes $\{\alpha_S^m\}_{m\in\{1,...,M_S\}}$ and $\{\alpha_F^m\}_{m\in\{1,...,M_F\}}$, respectively. Let Δt_S denote the timestep in the allegedly faster propagating solid and $\Delta t_F \gg \Delta t_S$ in the fluid. We propose a multilevel timestepping method that preserves the timestep size required by each solver, i.e. avoiding unnecessary time steps.

The MLTS procedure is sketched in Figure 2. It performs as follows: the solver for the solid material performs timesteps until the time of the first RK-stage of the fluid is reached. Next, the two solvers are synchronised by computing the RK-stage in the fluid (dashed line). The calculations in the solid proceed until the next RK-stage in the fluid is met (solid line). Each RK-stage demands for information at the boundary, especially for coupling conditions at the interface computed by Algorithm 1. While computing the RK-stages for the solid the only known information from the fluid to start is by the most recent computed RK-stage. In order to preserve accuracy *substages* are introduced in the fluid cells adjacent to the interface, i.e. in the fluid boundary layer of the interface. Due to the CFL-condition information coming from the interface cannot pass the boundary layer. Still, this method introduces some discretisation error. This is due to the fact that the solution in the fluid apart from the boundary layer is assumed to be constant between two RK-stages. Algorithm 2 summarises the procedure.

Algorithm 2 MLTS for Coupled RKDG

1: $\Delta t_S \leftarrow \text{GETDT}(solid)$

2: $\Delta t_F \leftarrow \text{GETDT}(fluid)$

3: **if** $\Delta t_S < \min_m(\alpha_F^m)\Delta t_F$ **then**

4:      $\Sigma_S \leftarrow \Delta t_S$ ▷ Total time passed in solid

5:      **for** $m \in \{1, \ldots, \texttt{M}_\texttt{F}\}$ **do**

6:          **while** $\Sigma_S \leq \alpha_F^m \Delta t_F$ **do**   ▷ As long as solid has not met the next RK-stage in fluid

7:             **for** $k \in \{1, \ldots, \texttt{M}_\texttt{S}\}$ **do**   ▷ Calculate RK-stages in solid

8:                Call $\text{RK-STAGE}(solid)$ ▷ Evaluate coupling conditions to obtain boundary conditions

9:                Call $\text{SUBSTAGE}(fluid)$ ▷ Evaluate coupling conditions to obtain boundary conditions

10:             **end for**

11:             $\Delta t_S \leftarrow \min\{\text{GETDT}(solid), \alpha_F^m \Delta t_F - \Sigma_S\}$

12:             $\Sigma_S \leftarrow \Sigma_S + \Delta t_S$

13:          **end while**   ▷ Now solid has reached the k-th RK stage of fluid

14:          $\Sigma_S \leftarrow 0$ ▷ Next stage

15:          Call $\text{RK-STAGE}(fluid)$ ▷ Evaluate coupling conditions to obtain boundary conditions

16:      **end for**

17: **else**   ▷ optimisation possible

18:      $\Delta t_F \leftarrow \min\{\Delta t_F, \Delta t_S\}$

19:      $\Delta t_S \leftarrow \Delta t_F$

20:      synchronised calculations

21: **end if**

---

4   Numerical Experiments

In order to solve the coupled problem consisting of the linear elastic model and the compressible Euler equations we apply to both systems a RKDG method [12]. The performance is enhanced by local multi-resolution based grid adaptation, see [13]. Details can be found in [8, 14]. The solver is implemented in the MULTIWAVE library [15]. The coupling procedure is carried out by computing the intersection of particular Lax curves of the linear elastic system and the Euler equations at the interface according to Algorithm 1. Whereas in [1] we used a synchronised timestepping procedure at the interface, we now apply our new multilevel timestepping procedure given by Algorithm 2. So far, it has only been implemented for one-dimensional spatial domains.

For the solid solver and the fluid solver we apply a third order DG scheme using polynomial elements of order $p = 3$ and a third-order SSP-Runge-Kutta method with three stages for the time-discretisation [16]. Both solvers use the same numerical flux, applied in the *interior* of each domain, and limiter, namely, the local Lax-Friedrichs flux and the minmod limiter from [12]. The synchronised timestepping procedure is compared to the multilevel timestepping procedure.

For our computations we choose plastic and stainless steel with parameters as in Table 1 for the linear elastic model. For the fluid we consider air with material parameters for the ideal gas $\gamma = 1.4$ and $c_v = 717.5 \; J/(kg \cdot K)$.

parameter	plastic	steel
density $\overline{\rho}\ [\ kg/m^3]$	1226	7800
Lamé constant $\lambda\ [N/m^2]$	1.4093×10^9	9.3288×10^{10}
Lamé constant $\mu\ [N/m^2]$	1.4093×10^9	9.3288×10^{10}
dilatation wave velocity $\overline{c}_1\ [m/s]$	1857.02	5990
shear wave velocity $\overline{c}_2\ [m/s]$	1072.15	3458

Table 1: Material parameters.

Having cavitation phenomena in mind we simulate a shock in the fluid moving towards the solid. The computational domain is $\Omega_S = [0, 1]\ m$ for the linear elastic system and $\Omega_F = [1, 2]\ m$ for the Euler system. In each domain we use a base grid of 50 cells and $L = 10$ levels of refinement. Thus, the uniformly refined grid would consist of 50×2^{10} cells that are never used in the course of the computation. However, due to grid adaptation the locally refined grids consist of about 100 cells. The CFL number is set to 0.1 and the final time is $T = 20\mu s$ for plastic and $T = 10\mu s$ for steel. For the linear elastic material we use uniform initial data $\overline{\mathbf{u}}_L$ in Ω_S for both plastic and steel. In Ω_F we set up a Riemann problem at $x^* = 1.025$ with data $\mathbf{u}_1$ in $\{x \in \Omega_F : x < x^*\}$ and $\mathbf{u}_2$ in $\{x \in \Omega_F : x \geq x^*\}$. The data is listed in Table 2.

Plastic or Steel		Fluid		
	$\overline{\mathbf{u}}_L$		$\mathbf{u}_1$	$\mathbf{u}_2$
$\overline{v}_1\ [m/s]$	0.0	$v_1\ [m/s]$	0.0	-27.6
$\overline{\sigma}_{11}\ [N/m^2]$	-100000	$p\ [N/m^2]$	100000	111864.4
		$\rho\ [kg/m^3]$	1.2	1.3

Table 2: Initial data for 1D validation test case.

To validate the coupling condition for the steel case we present in Figure 3 the negative stress $-\overline{\sigma}_{1,1}$ and the pressure p in the elastic material and the gas, respectively. The velocities $\overline{v}_1$ and v_1 perform analogously and, thus, are not shown here. We note that the velocities as well as the negative stress and the pressure are continuous at the interface located at $x = 1\ m$ confirming the coupling conditions (7). For the plastic case the results are similar and are omitted here.

We have performed several computations with increasing spatial and temporal resolution by a factor two with each additional refinement level. In Figure 4 and in Figure 5 we summarise the convergence behaviour for the plastic and steel case, respectively. The error is computed separately in the elastic material and the fluid where the L_1-error is computed as $\int_\Omega |u_L(x) - u(x)| dx$ with u_L and u denoting the DG solution for refinement level L and the exact solution, respectively. Additionally, we compute the empirical order of convergence EoC $= -\log_2(e_{L+1}/e_L)$ from the error.

For the steel case one can observe that the MLTS timestepping procedure adds to the discretisation error while in the case of plastic MLTS reduces the L_1-error. The EoC is about 0.95 for both the solid and the fluid part of the plastic case and about 1.0 for the
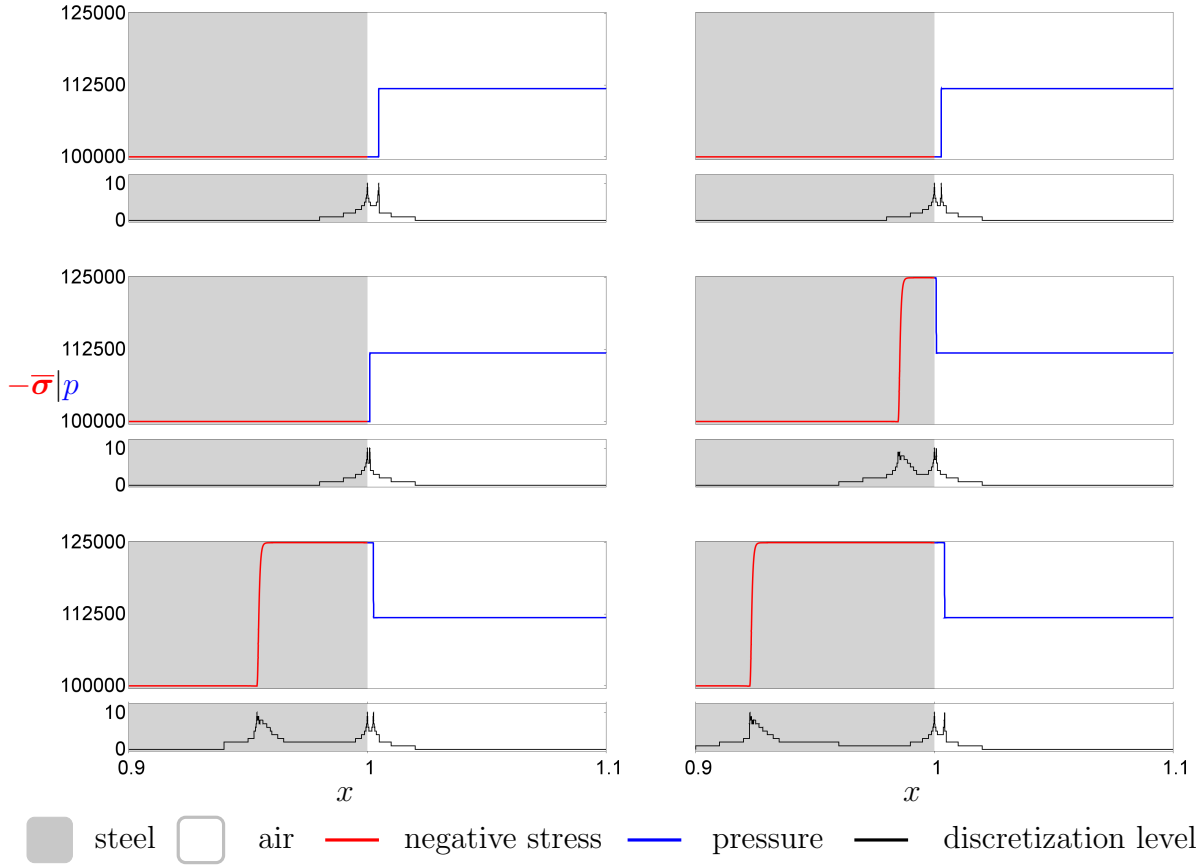
Figure 3: Pressure p (right) and negative stress $-\overline{\sigma}$ (left). Simulation of steel and air interaction, a shock in air (right) is moving towards the steel structure (left). From left to right, top to bottom the times presented are $t = 56.6\mu s, \ldots, 87.63\mu s$ equidistantly distributed. Below each timestep the local refinement discretisation level l of each cell is plotted. The cell width is 50×2^{-l}, i.e. the higher the level the smaller the cell.

steel case. Hence, applying the MLTS timestepping does not harm the convergence *order* in our test cases.

Since the solution exhibits discontinuities, the order of convergence in the L_1-norm is typically smaller than 1. For scalar one-dimensional conservation laws rigorous a-priori error estimates provide a convergence order of 0.5, e.g., [17, 18].

We observe that the MLTS timestepping procedure saves about 90% of the timesteps in the fluid compared to the synchronised method for plastic and about 95% for stainless steel.
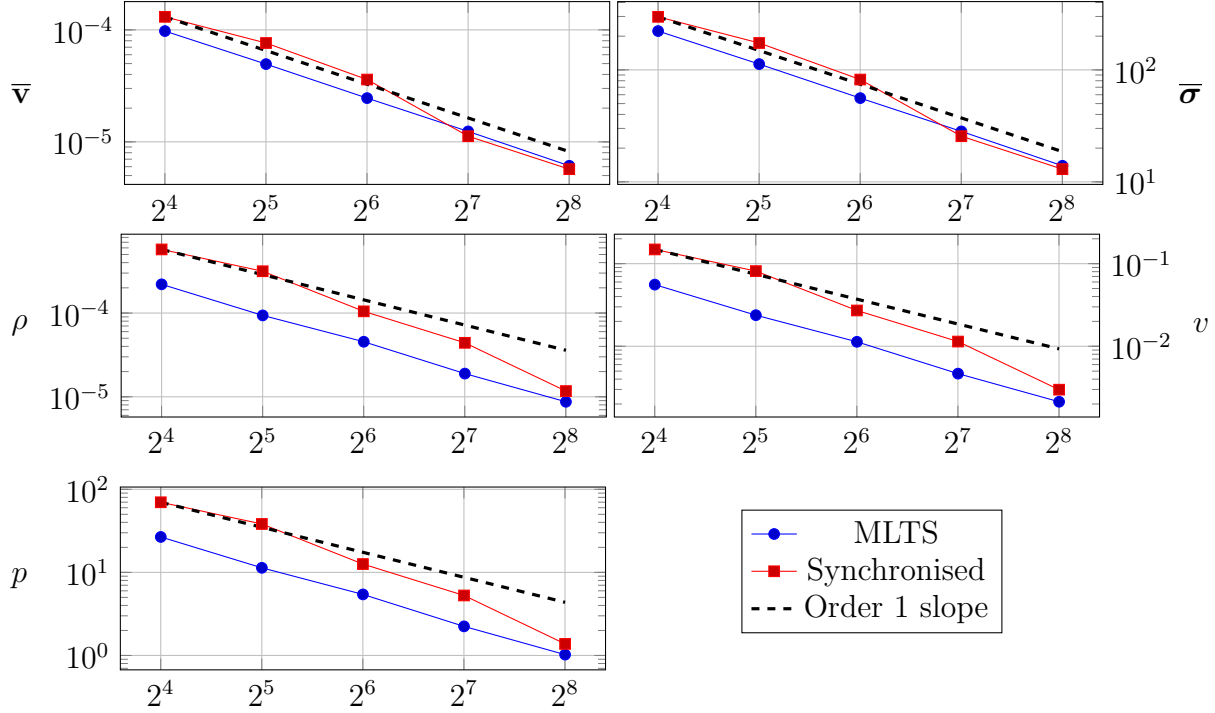
Figure 4: Convergence behaviour of plastic and air. On the vertical axes: L_1-error of the respective variable (from left to right, top to bottom: $\overline{\mathbf{v}}, \overline{\boldsymbol{\sigma}}, \rho, v, p$. On the horizontal axis: maximal refinement factor, i.e. corresponding maximal number of cells is 50×2^l where $l \in \{4, 5, \ldots, 8\}$.
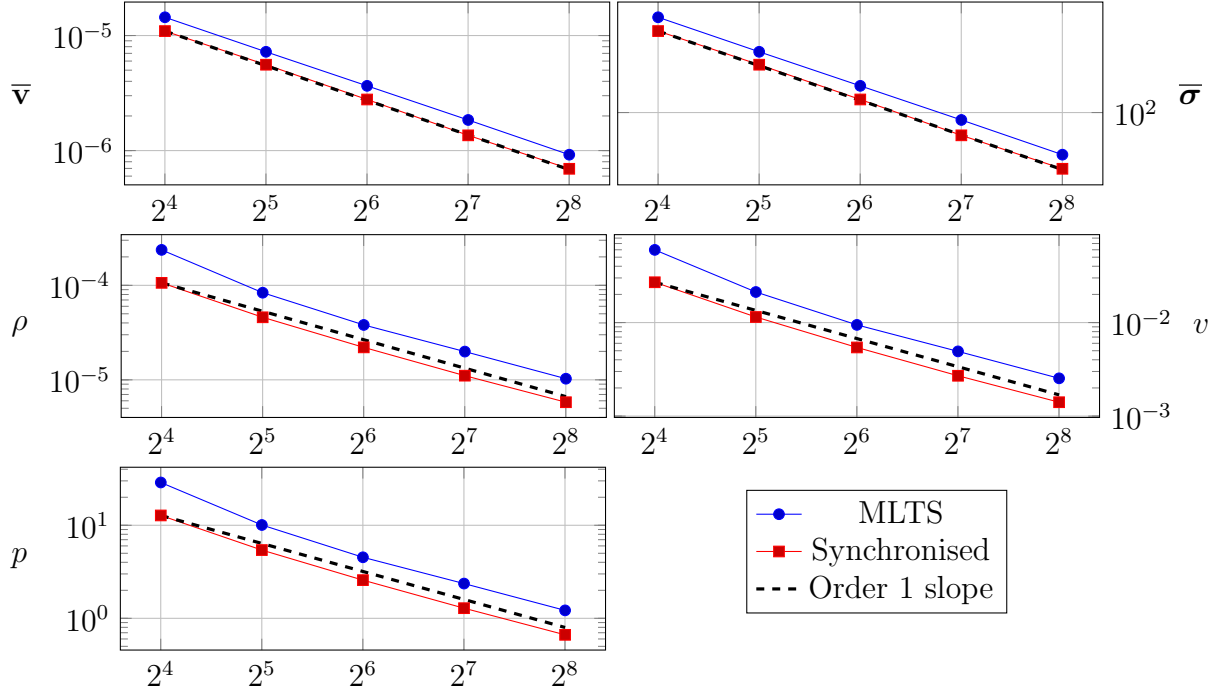
Figure 5: Convergence behaviour of steel and air. On the vertical axes: L_1-error of the respective variable (from left to right, top to bottom: $\overline{\mathbf{v}}, \overline{\boldsymbol{\sigma}}, \rho, v, p$. On the horizontal axis: maximal refinement factor, i.e. corresponding maximal number of cells is 50×2^l where $l \in \{4, 5, \ldots, 8\}$.

5   Outlook

In this work the MLTS procedure was implemented for a one-dimensional spatial domain. It will be extended to 2D and 3D in the future. For the more realistic scenario of cavitation damaging the coupling procedure has to be extended where instead of an ideal gas we use a stiffened gas in the compressible Euler equations.

A drawback in Algorithm 2 is the assumption that the timestep in the linear elastic model solver has to be less than one RK-stage of the fluid model. If this assumption is violated Algorithm 2 does not use MLTS but the synchronised timestepping. Applying a simple optimisation procedure for selecting a timestepping method would render this assumption unnecessary.

Finally, a consistency analysis is required in order to investigate the additional error introduced by the MLTS.

REFERENCES

[1] M. Herty, S. Müller, N. Gerhard, G. Xing, and B. Wang, "Fluid-structure coupling of linear elastic model with compressible flow models," *Int. J. for Numerical Methods in Fluids*, vol. 86, pp. 365–391, 2018.

[2] A. Bressan, S. Canic, M. Garavello, M. Herty, and B. Piccoli, "Flow on networks: recent results and perspectives," *European Mathematical Society-Surveys in Mathematical Sciences*, vol. 1, no. 1, pp. 47–11, 2014.

[3] R. M. Colombo and C. Mauri, "Euler system for compressible fluids at a junction," *J. Hyperbol. Differ. Eq.*, vol. 5, no. 3, pp. 547–568, 2008.

[4] E. Godlewski, K.-C. Le Thanh, and P.-A. Raviart, "The numerical interface coupling of nonlinear hyperbolic systems of conservation laws. II. The case of systems," *M2AN Math. Model. Numer. Anal.*, vol. 39, no. 4, pp. 649–692, 2005.

[5] M. K. Banda, A. Haeck, and M. Herty, "Numerical discretization of coupling conditions by high-order schemes," *J. Sci. Comp.*, vol. 69, no. 1, pp. 122–145, 2016.

[6] C. Dickopp, R. Gartz, and S. Müller, "Coupling of elastic solids with compressible two-phase fluids for the numerical investigation of cavitation damaging.," *International Journal on Finite Volumes*, vol. 10, pp. 1–39, 2013. hal-01121991.

[7] H.-z. Tang and G. Warnecke, "High resolution schemes for conservation laws and convection-diffusion equations with varying time and space grids," *J. Comp. Math.*, pp. 121–140, 2006.

[8] N. Gerhard and S. Müller, "Adaptive multiresolution discontinuous Galerkin schemes for conservation laws: multi-dimensional case.," *Comp. Appl. Math.*, vol. 35, no. 2, pp. 321–349, 2016.

[9] R. Menikoff and B. Plohr, "The Riemann problem for fluid flows of real materials," *Rev. Mod. Phys.*, vol. 61, pp. 75–130, 1989.

[10] C. M. Dafermos, *Hyperbolic conservation laws in continuum physics*, vol. 325 of *Grundlehren der Mathematischen Wissenschaften [Fundamental Principles of Mathematical Sciences]*. Berlin: Springer-Verlag, second ed., 2005.

[11] M. K. Banda, M. Herty, and A. Klar, "Gas flow in pipeline networks," *Netw. Heterog. Media*, vol. 1, no. 1, pp. 41–56, 2006.

[12] B. Cockburn and C.-W. Shu, "The Runge-Kutta discontinuous Galerkin method for conservation laws V: multidimensional systems," *J. Comput. Phys.*, vol. 141, pp. 199–244, 1998.

[13] N. Hovhannisyan, S. Müller, and R. Schäfer, "Adaptive multiresolution discontinuous Galerkin schemes for conservation laws.," *Math. Comput.*, vol. 83, no. 285, pp. 113–151, 2014.

[14] N. Gerhard, F. Iacono, G. May, S. Müller, and R. Schäfer, "A high-order discontinuous Galerkin discretization with multiwavelet-based grid adaptation for compressible flows.," *J. Sci. Comput.*, vol. 62, no. 1, pp. 25–52, 2015.

[15] S. Müller and A. Sikstel, "Multiwave," 2018. Technical Report, `https://www.igpm.rwth-aachen.de/multiwave`, [Online; accessed 30-April-2018].

[16] S. Gottlieb, C.-W. Shu, and E. Tadmor, "Strong stability-preserving high-order time discretization methods," *SIAM Rev.*, vol. 43, pp. 89–112, 2001.

[17] D. Kröner, *Numerical schemes for conservation laws*. Wiley-Teubner Series Advances in Numerical Mathematics, Chichester: Wiley. Stuttgart: Teubner, 1997.

[18] B. Cockburn and C.-W. Shu, "TVB Runge-Kutta local projection discontinuous Galerkin finite element method for conservation laws II: General framework.," *Math. Comp.*, vol. 52, pp. 411–435, 1989.